



Springer

Dear Author:

Please find attached the final pdf file of your contribution, which can be viewed using the Acrobat Reader, version 3.0 or higher. We would kindly like to draw your attention to the fact that copyright law is also valid for electronic products. This means especially that:

- You may print the file and distribute it amongst your colleagues in the scientific community for scientific and/or personal use.
- You may make your article published by Springer-Verlag available on your personal home page provided the source of the published article is cited and Springer-Verlag and/or other owner is mentioned as copyright holder. You are requested to create a link to the published article in Springer's internet service. The link must be accompanied by the following text: "The original publication is available at springerlink.com". Please use the appropriate DOI for the article. Articles disseminated via SpringerLink are indexed, abstracted and referenced by many abstracting and information services, bibliographic networks, subscription agencies, library networks and consortia.
- Without having asked Springer-Verlag for a separate permission your institute/your company is not allowed to place this file on its homepage.
- You may not alter the pdf file, as changes to the published contribution are prohibited by copyright law.
- Please address any queries to the production editor of the journal in question, giving your name, the journal title, volume and first page number.

Yours sincerely,

Springer-Verlag

M. Walgreen · Huib E. de Swart · D. Calvete

A model for grain-size sorting over tidal sand ridges

Received: 31 October 2002 / Accepted: 17 October 2003
© Springer-Verlag 2004

Abstract. A model was developed and analyzed to quantify the effect of graded sediment on the formation of tidal sand ridges. Field data reveal coarse (fine) sediment at the crests (in the troughs), but often phase shifts between the mean grain-size distribution and the bottom topography occur. Following earlier work, this study is based on a linear stability analysis of a basic state with respect to small bottom perturbations. The basic state describes an alongshore tidal current on a coastal shelf. Sediment is transported as bed load and dynamic hiding effects are accounted for. A one-layer model for the bed evolution is used and two grain size classes (fine and coarse sand) are considered. Results indicate an increase in growth and migration rates of tidal sand ridges for a bimodal mixture, whilst the wavelength of the ridges remains unchanged. A symmetrical externally forced tidal current results in a grain-size distribution which is in phase with the ridges. Incorporation of an additional external M_4 tidal constituent or a steady current results in a phase shift between the grain-size distribution and ridge topography. These results show a general agreement with observations. The physical mechanism responsible for the observed grain-size distribution over the ridges is also discussed.

Keywords Tidal sand ridges · Grain-size distribution · Linear stability · Coastal shelf · Morphodynamics

Responsible Editor: Jens Kappenberg

M. Walgreen · H.E. de Swart (✉)
Institute for Marine and Atmospheric Research,
Utrecht University, Princetonplein 5,
3584CC Utrecht, The Netherlands
e-mail: H.E.deSwart@phys.uu.nl
Fax: +31 30 2543163

D. Calvete
Department de Física Aplicada,
Universitat Politècnica de Catalunya,
08034 Barcelona, Spain

1 Introduction

Offshore tidal sand ridges are rhythmic bedforms that are observed on the outer part of meso-tidal shelves (Off 1963). A characteristic spacing between successive crests is 5–8 km and the ridges are rotated cyclonically with respect to the dominant tidal current (Dyer and Huntley 1999). These characteristics have been explained in various studies dealing with tide–topography interaction (Zimmerman 1981; Huthnance 1982; Pattiaratchi and Collins 1987). One aspect that has not been addressed so far is the role of graded sediment in the morphodynamics of tidal sand ridges. Analysis of field observations indicates the potential importance of graded sediment: a persistent spatial variation of the surficial sediments over these ridges is found. A well-documented example of a tidal sand ridge is the Middelkerke Bank along the Belgian coast (see, for example, Lanckneus et al. 1994; Houthuys et al. 1994; Vincent et al. 1998). For the location of this bank on the Belgian shelf, see Fig. 1. The distribution of the mean grain size shows coarser sediment on the crests and a finer sediment in the troughs. Moreover, the location of the coarsest sediment is shifted seaward at the northern end of the Middelkerke Bank and landward at the southern end (Trentesaux et al. 1994). Data gathered from the more seaward located Kwinte Bank (Gao et al. 1994) indicate a similar grain-size pattern, with the seaward flank typically consisting of coarser sediment than the landward flank. Also for the more onshore located coastal banks a variation in the mean grain size is found (see Van Lancker 1999), with the coarsest sediments on the steep landward flank.

Sorting of sediment is also observed over other large-scale bedforms, such as shoreface-connected ridges, located along the east coast of the USA, on the Argentine shelf (Swift et al. 1978) and along the German coast (Antia 1996). Also, sorting is observed over sea ripples and alternate bars in rivers, see the review by Seminara

(1995). A theory that was able to explain the observed sorting characteristics over sea ripples was developed by Foti and Blondeaux (1995). This theory was based on a stability analysis of a morphodynamic model that involves transport of sediment with different grain sizes and that accounts for effects of dynamic hiding. The latter means that small grains effectively experience a smaller shear stress because they are hidden in between coarser grains. The findings of Foti and Blondeaux (1995) (coarse sand on the crests, fine sand in the troughs) turn out to be in agreement with field and laboratory data. Lanzoni and Tubino (1999) applied the concepts of linear stability to study the development of alternate bars and the grain-size distribution over them. Their model results are in qualitative agreement with experimental findings which show a reduced height, wavelength and migration of the bars with respect to the uniform sediment case. Also the sorting pattern, with coarse sediment prevailing on the upstream flank of the bar crest, is reproduced in their model. Walgreen et al. (2003) studied the sorting characteristics over shoreface-connected sand ridges on storm-dominated shelves. They showed that including a size-dependent suspended sediment flux is essential to reproduce the observed mean grain-size pattern, with the coarser sediment on the upcurrent flank of the ridges.

The first objective of the present study was to gain understanding of the physical mechanisms responsible for the observed grain-size distribution over the tidal sand ridges. In addition, the work was aimed at identifying possible causes for the shift between the crest and the maximum in the mean grain-size. The second objective was to investigate the influence of sediment sorting on the temporal (i.e. growth and migration) and spatial characteristics of the ridges. Following earlier

work, it is hypothesized that tidal sand ridges form as a free instability of a morphodynamic system. Calvete et al. (2001) studied the initial formation of tidal sand ridges in the case of uniform sediment. In contrast to the open domain, as was used in earlier studies by Huthnance (1982) and Hulscher et al. (1993), the shelf is bounded by a coast. In the present paper the model is extended with a formulation for the transport of a sediment mixture. The approach is similar to that used by Walgreen et al. (2003), who investigated the effect of sediment sorting on the formation of other large-scale bedforms detected on coastal shelves. The model for tidal sand ridges differs from the one presented by Walgreen et al. (2003) in the sense that the dominant forcing is by tides, rather than by storms, and that suspended load transport is neglected.

In Section 2 a brief description of the model is given, including the linear stability approach to solve the equations. Section 3 shows the influence of a bimodal sediment mixture, as compared to sediment with a single grain-size, on the initial formation of tidal sand ridges. A physical interpretation of the model results is presented in Section 4, followed by a comparison with field observations. In this last section, the conclusions are given.

2 Model formulation and solution methods

A local model is used to investigate the flow–topography interaction on a tide-dominated coastal shelf. To this end, it is assumed that bedforms can develop as perturbations on an alongshore-uniform basic state, as defined in Section 3. The geometry of the model represents a semi-infinite domain, bounded on the landward side by the transition from the shoreface to the (sloping) inner shelf. Further seaward, a flat bottom is used to represent the outer shelf, see Fig. 2. For more details on the formulation of the model, see Walgreen et al. (2002).

2.1 Hydrodynamics

The water motion is described by the depth-averaged (2DH) shallow water equations.

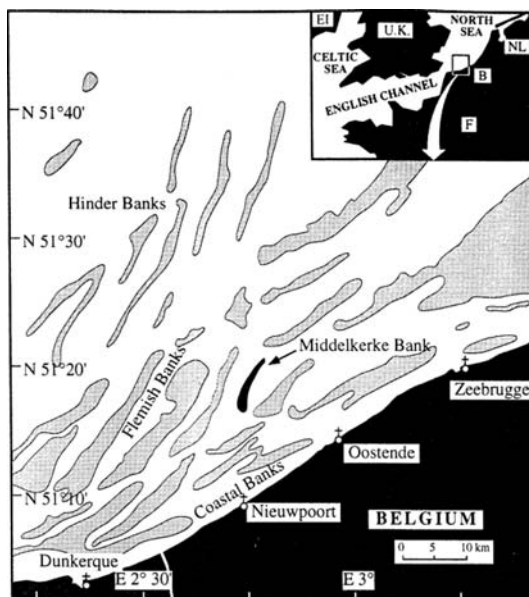


Fig. 1 Sketch of the ridges on the Belgian shelf. The location of the Middelkerke Bank is indicated, which is one of the tidal sand ridges in the group of ridges referred to as the Flemish Banks. (Trentesaux et al. 1999)

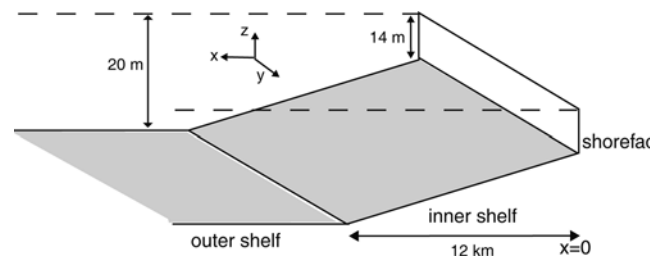


Fig. 2 Sketch of the geometry of the model, representing the inner shelf and part of the outer shelf of a coastal sea

$$\frac{\partial \mathbf{v}}{\partial t} + (\mathbf{v} \cdot \nabla) \mathbf{v} + f \mathbf{e}_z \times \mathbf{v} = -g \nabla z_s - \frac{\tau_b}{\rho D} \quad (1)$$

$$\frac{\partial D}{\partial t} + \nabla \cdot (D \mathbf{v}) = 0. \quad (2)$$

Here \mathbf{v} is the depth- and wave-averaged velocity, f is the Coriolis parameter, \mathbf{e}_z a unit vector in the vertical direction, g the acceleration due to gravity, ρ is the density, $\tau_b = \rho r \mathbf{v}$ is a linearized bed shear stress, t is time and ∇ the horizontal nabla operator. The bottom friction coefficient is $r = c_d U \sim 10^{-3} \text{ ms}^{-1}$, where c_d is the drag coefficient and U a characteristic value for the depth-averaged velocity. In this paper results will be presented for a bottom friction coefficient that is independent of the grain size. The local water depth is given by $D = z_s - z_b \simeq -z_b$, where z_s is the free-surface elevation and z_b is the bottom depth. A rigid lid is assumed, which also implies that the first term in Eq. (2) can be omitted. This is justified on the basis of a small Froude number. The main forcing in the momentum equations is due to a prescribed pressure gradient induced by a tidal wave propagating along the coast.

2.2 Sediment dynamics

A sediment mixture consisting of N different grain-size classes d_i can be described using a logarithmic scale, the phi scale:

$$d_i = 2^{-\phi_i} \quad \text{or} \quad \phi_i = -\log_2 d_i,$$

where d_i is measured in units of mm. The mean grain size and the standard deviation are defined as

$$\phi_m = \sum_{i=1}^N \phi_i \mathcal{F}_i \quad \sigma^2 = \sum_{i=1}^N (\phi_i - \phi_m)^2 \mathcal{F}_i.$$

Here, \mathcal{F}_i is the probability distribution function of the grain-size class i and obeys the constraint $\sum_{i=1}^N \mathcal{F}_i = 1$.

The hydrodynamic equations discussed in Section 2.1 are supplemented with a sediment transport formulation, based on the concepts introduced by Bailard (1981) for bed load transport on a sloping bottom. In turn, the evolution of the bottom results from a convergence or divergence in the sediment flux. A one-layer model for the bed, based upon the concept of an active transport layer overlaying an inactive substrate is used (see Ribberink 1987; Seminara 1995). The active layer is well mixed and has a thickness of L_a , in the order of 2–3 mm. The exchange of sediment with the substrate is ignored. Consequently, the relation between the bottom evolution, the grain-size evolution and the sediment flux of class d_i yields

$$(1-p) \left(\mathcal{F}_i \frac{\partial z_b}{\partial t} + L_a \frac{\partial \mathcal{F}_i}{\partial t} \right) = -\nabla \cdot \overline{\mathbf{q}_{bi}}. \quad (3)$$

In Eq. (3), \mathbf{q}_{bi} is the volumetric flux per unit width of grains of diameter d_i and $p \sim 0.4$ is the porosity of the

bed. The first term on the left-hand side of Eq. (3) represents the bottom changes, and the second describes changes in the sediment distribution in the active layer. Besides, the formation of tidal sand ridges takes place on a time scale which is much larger than the hydrodynamic time scale. For instance, Vincent et al. (1998) estimated the time scale for the growth of the Middelkerke Bank to be 10^2 – 10^3 years. Therefore, a tide- and wave-averaged sediment flux is used, denoted by the overbar, and the flow adjusts instantaneously to the new bottom.

Tides are supposed to control the growth of tidal sand ridges. This is supported by the findings of Trenetiaux et al. (1994), which show a near-absence of wave-induced structures on the Middelkerke Bank. This implies that bed load is the dominant mode of transport and suspended load contributions can be neglected. A more elaborate discussion on this topic is given in Section 4.3. In case of a single grain size, the (wave-averaged) bed load transport reads

$$\mathbf{q}_b = v_b |\mathbf{v}|^3 \left[\frac{\mathbf{v}}{|\mathbf{v}|} - \lambda_b \nabla h \right],$$

where $v_b \sim 4 \times 10^{-4} \text{ s}^2 \text{ m}^{-1}$ is a coefficient, $\lambda_b \sim 1$ and h is the bottom level with respect to the alongshore-averaged bathymetry. Note that this flux is proportional to the velocity cubed, and that it includes effects due to the local slope of the bottom. To calculate the sediment flux of a specific grain-size within a sediment mixture, two additional corrections are made, such that

$$\mathbf{q}_{bi} = \mathcal{F}_i \mathcal{G}_{bi} \mathbf{q}_b.$$

Firstly, \mathcal{F}_i corrects for the availability of grains of diameter d_i in the mixture. Secondly, dynamic ‘‘hiding’’ effects are included, represented by the function \mathcal{G}_{bi} . This is the bed load transport capacity function for sediment of grain-size d_i , and accounts for the effect that finer grains experience a less intense fluid drag than coarser grains. It is convenient to use the expression

$$\mathcal{G}_{bi} = \left(\frac{d_i}{d_m} \right)^{c_b}, \quad (4)$$

with the exponent c_b measuring the influence of the hiding on the transport of sediment. A default value of $c_b = 0.75$ is used (see discussion in Walgreen et al. 2003), which results in a reduced transport rate of the grain sizes finer than the mean grain size. At the landward and seaward boundaries of the model domain, no cross-shore velocity component and no bottom changes are allowed.

2.3 Basic state

The possible onset of bedforms as free morphodynamic instabilities, which evolve on a basic state of the water-bottom system, is investigated. The model allows for a morphodynamic equilibrium, which is alongshore-uniform:

$$\mathbf{v} = [0, V(x, t)] \quad z_b = -H(x) \quad z_s = s(t)y + z_{s0}(x, t)$$

$$\mathcal{F}_i = F_i \quad \phi_m = \Phi_m \quad \sigma = \sigma_0 .$$

It describes a shore-parallel current $V(x, t)$ over a fixed bottom $z_b = -H(x)$. The grain-size distribution function F_i of the basic state can have an arbitrary structure in the x direction. For simplicity, F_i is assumed to be independent of this coordinate. As a result, the mean grain-size Φ_m and the standard deviation σ_0 are also uniform in the domain. The velocity of the basic state is a solution of the alongshore momentum Eq. (1):

$$\frac{\partial V}{\partial t} = -gs - \frac{rV}{H} .$$

The alongshore gradient in the free surface, s , is defined by a steady component s_0 and two oscillatory components:

$$s \equiv s_0 - s_1 \cos(\omega t) - s_2 \cos(2\omega t + \theta) .$$

Here, s_1 and s_2 are the amplitudes of the sea-surface gradients with the frequency ω of the M_2 and with frequency 2ω of the M_4 tide, respectively. Furthermore, θ is a (constant) phase between the two tidal harmonics. The velocity of the basic state consists of a steady component, V_0 , and an oscillatory component, due to the M_2 and M_4 tidal wave:

$$V(x, t) = V_0(x) + V_{M_2}(x) \sin[\omega t + \varphi_{M_2}(x)]$$

$$+ V_{M_4}(x) \sin[2\omega t + \varphi_{M_4}(x) + \theta] , \quad (5)$$

where

$$V_0(x) = -\frac{gs_0 H}{r} . \quad (6)$$

The cross-shore profile of the tidal current amplitudes and phases are given by:

$$V_{M_2}(x) = \frac{gs_1 H}{\sqrt{(\omega H)^2 + r^2}} \quad \varphi_{M_2}(x) = \arctan\left(\frac{r}{H}\right)$$

$$V_{M_4}(x) = \frac{gs_2 H}{\sqrt{(2\omega H)^2 + r^2}} \quad \varphi_{M_4}(x) = \arctan\left(\frac{r}{2H}\right) .$$

The values used for the basic state variables are given in Sect. 3.1.

2.4 Stability analysis

The dynamics of small perturbations on this basic state are studied. In the case of a positive feedback between the flow and the bottom perturbation, the basic state is unstable and rhythmic bottom features will develop. Solutions of the form

$$\mathbf{v} = [0, V(x, t)] + [u'(x, y, t), v'(x, y, t)]$$

$$z_s = s(t)y + z_{s0}(x, t) + \eta'(x, y, t)$$

$$z_b = -H(x) + h(x, y, t)$$

$$\mathbf{q}_b = \mathbf{q}_{b0}(x) + \mathbf{q}'_b(x, y, t)$$

$$\mathcal{G}_{bi} = G_{bi} + g_{bi}(x, y, t)$$

$$\mathcal{F}_i = F_i + f_i(x, y, t)$$

$$\phi_m = \Phi_m + \phi'_m(x, y, t)$$

$$\sigma = \sigma_0 + \sigma'(x, y, t)$$

$$L_a = L_{a0} + L'_a(x, y, t)$$

are substituted in the equations of motion and the results are linearized. In this paper, a two-size sediment mixture will be used, where d_1 (or ϕ_1) and d_2 (or ϕ_2) represent the sizes of the fine and coarse grains, respectively. The constraint on the grain-size fraction becomes

$$F_1 + F_2 = 1 \quad f_1 = -f_2 . \quad (7)$$

The mean grain-size and the standard deviation in the basic state simplify to

$$\Phi_m = \phi_1 F_1 + \phi_2 F_2 \quad \sigma_0^2 = F_2 F_1 (\phi_1 - \phi_2)^2 .$$

From these expressions the values of the grain diameters of the fine and coarse size classes on the ϕ scale, i.e. ϕ_1 and ϕ_2 , can be obtained as a function of Φ_m , σ_0 and F_1 . Together with the relationships given above, the perturbations in the mean grain-size and standard deviation can be written as

$$\phi'_m = \frac{\sigma_0}{\sqrt{F_2 F_1}} f_1 \quad \sigma' = \frac{\sigma_0(F_2 - F_1)}{2F_2 F_1} f_1 .$$

The linearized form of the bottom evolution Eq. (3) is

$$F_i \frac{\partial h}{\partial t} + L_{a0} \frac{\partial f_i}{\partial t} = -\nabla \cdot \overline{\mathbf{q}'_{bi}} , \quad (8)$$

where

$$\mathbf{q}'_{bi} = F_i G_{bi} \mathbf{q}'_b + \mathbf{q}_{b0} (G_{bi} f_i + F_i g_{bi}) \quad (9)$$

is the perturbed bed load flux and \mathbf{q}_{b0} , \mathbf{q}'_b and $\nabla \cdot \mathbf{q}'_b$ are given in the Appendix. The active layer thickness in the basic state is given by $L_{a0} = d_m 2^{\sigma_0}$ and from Eq. (4) it follows that

$$G_{bi} = 2^{c_b(\Phi_m - \phi_i)} \quad g_{bi} = c_b \ln 2 G_{bi} \phi'_m . \quad (10)$$

Summation of Eq. (8) over the two fractions and using the constraint (7) for the probability distribution, results in an equation relating the bottom evolution to the sum of the sediment flux over all grain sizes. Back-substitution of this result in Eq. (8) yields the evolution of the distribution function f_i . The final results are

$$(1-p) \frac{\partial h}{\partial t} = -[\nabla \cdot \overline{\mathbf{q}'_{b1}} + \nabla \cdot \overline{\mathbf{q}'_{b2}}] \quad (11)$$

$$(1-p) L_{a0} \frac{\partial f_1}{\partial t} = F_1 \nabla \cdot \overline{\mathbf{q}'_{b2}} - F_2 \nabla \cdot \overline{\mathbf{q}'_{b1}} . \quad (12)$$

The solution of any perturbed variable is sinusoidal in the alongshore direction (with wavenumber k), and exponential in time (with complex frequency Ω). In

particular, the bottom perturbations are topographic waves propagating along the shelf, being of the form

$$h(x, y, t) = \text{Re} \left\{ \hat{h}(x) e^{iky + \Omega t} \right\}.$$

A similar expression holds for f_1 . The stability analysis yields for each wavenumber k solutions for Ω and the corresponding cross-shore structures of the perturbed variables, also called modes. The real part Ω_r of Ω is the growth rate, with Ω_r^{-1} being the e-folding time-scale. Furthermore, its imaginary part Ω_{im} is the frequency. The migration velocity of the perturbation is $c = -\Omega_{im}/k$. Of specific interest are growing perturbations, which satisfy $\Omega_r > 0$. The preferred mode is defined as the mode with the largest growth rate. From the boundary conditions it follows that $u' = 0$ and $h = 0$ at the transition from the shoreface to the inner shelf ($x = 0$) and at $x \rightarrow \infty$. Solutions of the linear stability problem were obtained by numerical methods, for details see Calvete et al. (2001) and references therein.

3 Results

The model was run for different parameter settings to meet the objectives of this study (see Sect. 1). In particular, the sensitivity of the model results with respect to variations in the standard deviation of the mixture, the size distribution in the basic state and the exponent c_b in the hiding function for bed load was investigated. First, a brief consideration of the most important characteristics of a typical tide-dominated coastal shelf is given. The results presented in this section are based on these values.

3.1 Shelf characteristics

On the Belgian coastal shelf, different types of sand ridges are present; these can be grouped according to their orientation with respect to the coastline. The Flemish Banks, including the Middelkerke Bank, are tidal sand ridges located in a meso-tidal environment. A narrow coastal region of about 12 km in width separates the Flemish Banks from the coastline. The depth of the Middelkerke Bank varies from 4 m MLLWS (mean lowest low water at spring) at its crest up to 20 m in the adjacent channels (Trentesaux et al. 1994). To verify the model results, this meso-tidal shelf was used as a prototype. It is approximately 14 m deep at the transition from the shoreface to the inner shelf, 12 km wide and 20 m deep on the outer shelf (see Fig. 2). The latitude is 52°N , for which the Coriolis parameter $f \sim 1 \times 10^{-4} \text{ s}^{-1}$. Although the dominant hydrodynamical forcing is due to the M_2 tide, contributions of the M_4 constituent and residual currents are present. The behaviour of the tidal current changes from ebb-dominated to almost symmetrical

north of the Flemish Banks, to increasingly flood-dominated closer to the shore, with a residual flow directed towards the northeast (along a SW–NE-trending coastline, see Lanckneus et al. 1994). This pattern is in agreement with the residual sand transport, which is directed to the northeast in a narrow coastal region and to the southwest in the offshore region. On the scale of the Belgian shelf, measurements indicate an almost zero long-term average of the steady current (Lanckneus et al. 1994).

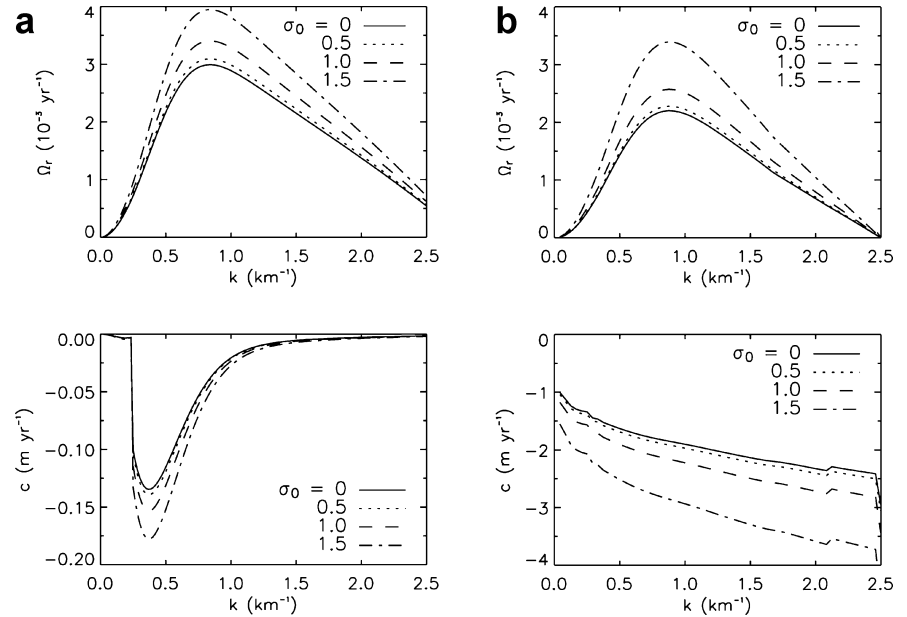
To investigate the effect of the characteristics of the externally forced velocity field on the formation of tidal sand ridges, different forcing conditions were considered. Firstly, a forcing by the M_2 tidal constituent was used, with a depth-averaged tidal current amplitude of 0.5 ms^{-1} . This means that the tidally averaged along-shore sediment transport is zero. Secondly, asymmetry in the flow was introduced by adding an M_4 constituent to the forcing, where $V_{M_2} \sim 0.45 \text{ ms}^{-1}$, $V_{M_4} \sim 0.05 \text{ ms}^{-1}$ (Williams et al. 2000). Lastly, an asymmetrical current, introduced by adding a steady component $V_0 \sim -0.05 \text{ ms}^{-1}$ (free surface forcing $s_0 \sim 4 \times 10^{-7}$) to the V_{M_2} component, was investigated. The former two situations are characterised by a net alongshore (flood-dominated) current and a tidally averaged sediment flux along the coast (in a northeasterly direction).

On the scale of the Belgian coastal shelf, the sediment becomes coarser offshore; locally, the coarsest mean grain-size is found on the crest of the ridges. For simplicity, in the basic state a uniform mean grain-size of $d_m = 0.35 \text{ mm}$ ($\Phi_m = 1.5$), characteristic of the surficial sediment on the Middelkerke Bank (Trentesaux et al. 1994), was adopted throughout the domain. The sediment size distribution observed on the steep seaward flank of the sand ridge supports the use of a bimodal sediment mixture: two peaks are present, for the size classes of 0.25–0.30 and 0.42–0.50 mm (Vincent et al. 1998). Thus, the mean grain-size used in the basic state of the model is closest to that observed on the steep flank. The diameters of the two size classes in the sediment mixture were confined to non-cohesive sediment in the sand range ($3 > \phi_i > 0$). Table 1 presents the properties of the sediment mixtures used in the different experiments.

Table 1 Parameter values for uniform and bimodal sediment, as used in the model experiments

	Uniform Fig. 3	Bimodal Fig. 3, 4, 5, 6	Bimodal Fig. 3	Bimodal Fig. 5
σ_0	0	0.5	1.0	0.4
F_1	1	0.5	0.5	0.8
F_2	0	0.5	0.5	0.2
Φ_m	1.5	1.5	1.5	1.8
ϕ_1	1.5	2.0	2.5	2.0
ϕ_2	1.5	1.0	0.5	1.0
d_1 (mm)	0.35	0.25	0.18	0.25
d_2 (mm)	0.35	0.50	0.71	0.50

Fig. 3 Growth rate Ω_r and migration velocity, c , of dominant cross-shore mode as a function of the alongshore wavenumber k for different values of the standard deviation and the same mean grain-size in all experiments ($\Phi_m = 1.5$). Forcing by the M_2 tide (a) and $M_2 + M_4$ tides (b) The coefficient in the hiding function is $c_b = 0.75$



3.2 Sensitivity to standard deviation

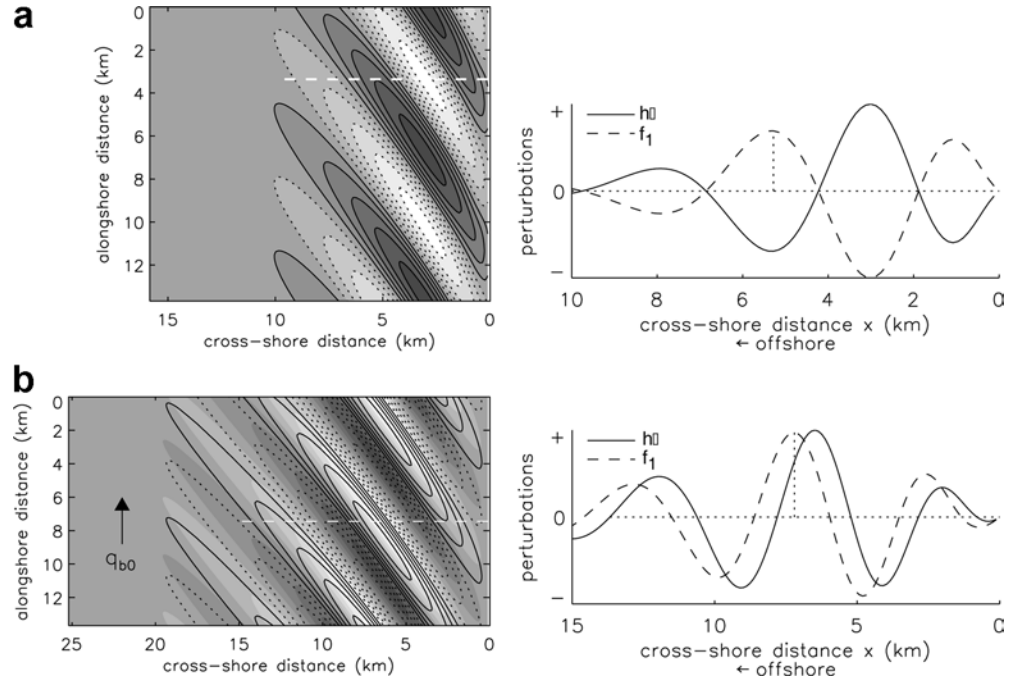
The growth rates and migration velocities of the preferred mode for different compositions of the sediment bed are shown in Fig. 3. The standard deviation σ_0 of the basic state increased from zero (i.e. uniform sediment) to a bimodal mixture, in the case of forcing by a pure M_2 tide and a combined M_2 , M_4 tide. A constant mean grain-size and equal weight percentages of the two size classes in the basic state ($F_1 = F_2 = 0.5$) are assumed. As a result, the grain sizes d_1 and d_2 change with σ_0 (see Table 1). For a bimodal mixture growth rates and migration speeds increase with increasing σ_0 . The wavelengths ($2\pi/k$) of the ridges for which maximum growth rates are attained remain unchanged: 7.5 and 7.2 km for M_2 and $M_2 + M_4$ tidal conditions, respectively. The corresponding e-folding time scales for the initial growth are 320 yr (M_2) and 440 yr ($M_2 + M_4$), for a value of $\sigma_0 = 0.5$. The tidal sand ridges migrate with a speed of 0.04 m yr^{-1} and 1.9 m yr^{-1} , in these two cases respectively. Compared to the situation of ridges on a horizontally flat bottom, the transverse bottom slope changes the residual circulation due to Coriolis and frictional torques. The result is a small non-zero migration velocity for a symmetrical (M_2) tidal forcing. In fact, the relative increase in growth and migration due to a changing standard deviation was larger for a combined M_2 and M_4 tide than for a symmetrical M_2 tide. Experiments were carried out with a velocity of the basic state consisting of a steady current V_0 and an M_2 tidal current. The results (not shown) indicate that growth rates and migration velocities again increase with σ_0 . The bedforms migrate in the direction of the mean flow. This behaviour is similar to that obtained in the case of an asymmetrical flow, driven by the M_2 and M_4 tidal constituents. In the situation where forcing includes both the M_4 tide and a steady component, it is possible

to have a migration of the bedforms against the direction of the steady current. Besio et al. (2003) used this combination of currents to explain the upcurrent-migration of sand waves. A necessary condition is that the phase between the M_2 and M_4 tide is such that it introduces a residual sediment transport in the direction opposite to the residual sediment transport caused by the residual current. In addition, for the case of tidal sand ridges the amplitude of the M_4 tide should be at least three to four times larger than the amplitude of the steady current. As such situations are not observed on the Belgian shelf, this is not further pursued.

The patterns of topographic perturbations (shaded) and variations in the mean grain-size are shown in Fig. 4, for parameter values of non-uniform sediment. The contour lines refer to the perturbation in the fraction of the finest grains: values along solid lines are positive and indicate a locally finer mean grain size. If a symmetrical tidal current is used, the grain-size distribution is in phase with the ridge topography, with the finest sediments located in the troughs. Incorporation of an additional M_4 tide in the forcing results in a phase shift between the mean grain-size and topography. In the present case of a flood-dominant tidal current (residual transport indicated by the arrow), the finest sediments are located on the upcurrent (seaward) flank and on the crests of the ridges. The underlying physics will be discussed in Sections 4.1 and 4.2.

In order to test the robustness of these results, experiments were carried out in which the diameters of both fractions were fixed and the standard deviation was varied. This implies the changing of the composition of the sediment mixture, i.e. the mean Φ_m and the fractions F_1 and F_2 of the sediment in the basic state will change. A linear relationship exists between Φ_m and F_1 : higher values of F_1 correspond to higher values of Φ_m (i.e. finer mean grain sizes). The results in Fig. 5 are shown only

Fig. 4a, b Bottom perturbations (grey scale: *light*, bars, *dark* troughs) and perturbations in the distribution of mean grain-size (solid lines finer; dashed lines coarser). Also shown is the variation of the bottom and mean grain-size along a cross-section (location indicated by white dashed line in the contour plots), positive (negative) values of f_1 indicate a local fining (coarsening) of the bottom sediment. Ridges are shown for $\sigma_0 = 0.5$, $\Phi_m = 1.5$, $c_b = 0.75$ and forcing by M_2 tide (a) and $M_2 + M_4$ tides (b)



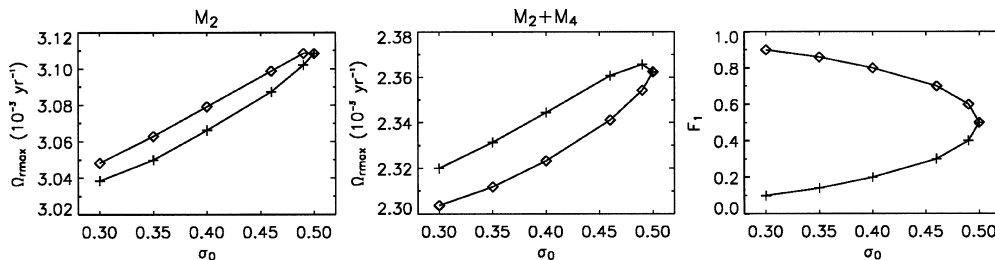
for the preferred mode (which has the largest growth rate). As before, the maximum growth rates and migration velocities (not shown) increase with the standard deviation. Wavelengths of the preferred mode do not change, and the perturbations in the bed and sediment distribution have the same characteristics as those shown in Fig. 4. In the case of $\sigma_0 < 0.5$, two different compositions of the sediment mixture are possible for each value of the standard deviation. One is indicated by diamonds and a high percentage of fine grains ($F_1 > 0.5$) and a mean grain-size $\Phi_m > 1.5$. The second with a high percentage of coarse grains ($F_2 > 0.5$ and $\Phi_m < 1.5$) is indicated by crosses. Figure 5 demonstrates that, in the case of forcing solely by an M_2 tidal current (left subplot), for a fixed value of σ_0 the instabilities grow fastest for a grain-size distribution in the basic state that contains more fine than coarse sediment. The opposite

occurs in case of a combined M_2 , M_4 tidal current (middle subplot).

3.3 Sensitivity to hiding coefficient

Another series of experiments was performed to investigate the influence of the intensity of the hiding in the bed load transport capacity function, as measured by the coefficient c_b , see Eq. (4). For all three velocity profiles (M_2 alone, $M_2 + M_4$ and $M_2 + M_0$) the maximum growth rates and corresponding migration of the preferred mode are shown in Fig. 6 as a function of c_b . The wavelength of the preferred mode does not depend on c_b . The experiments reveal enhanced growth rates and migration velocities for higher values of the exponent c_b , i.e. if dynamic hiding effects become stronger. Positive (negative) values of c_b correspond to a reduced (enhanced) bed load transport of fine grains, with respect to the coarse grains. The relative influence of hiding is larger for asymmetrical flows than for symmetrical flows. Apparently, an enhancement of both the growth and the migration of the ridges is present, irrespective of the sign of the hiding coefficient. This will be explained in the next section.

Fig. 5 Growth rate Ω_r of the preferred mode as a function of the standard deviation of the mixture σ_0 of the basic state. Forcing due to M_2 tide (left), and $M_2 + M_4$ tide (middle). The default value $c_b = 0.75$ is used. Results are shown for a bimodal mixture with fixed grain sizes $\phi_1 = 2.0$ and $\phi_1 = 1.0$, where changes in the basic state σ_0 result in variation of Φ_m and F_1 (right). Note that a larger weight percentage of ϕ_1 (i.e. $F_1 > 0.5$, indicated by diamonds), as well as a larger weight percentage of ϕ_2 ($F_1 < 0.5$, indicated by crosses) can result in the same value of σ_0



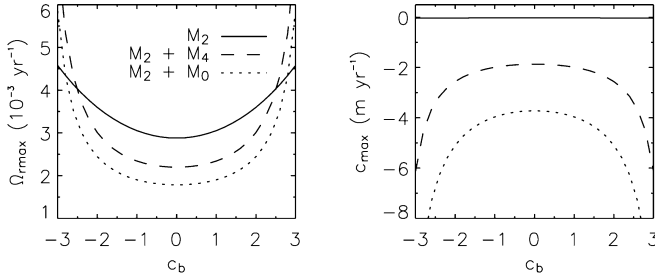


Fig. 6 Growth rate and migration velocity of the preferred mode as a function of the coefficient c_b , indicating the strength of the dynamic hiding. Results are shown for a current forced by M_2 tide $M_2 + M_4$ tide and M_2 tide + steady current (M_0). Other parameter values are: $F_1 = 0.5$, $\sigma_0 = 0.5$, $\Phi_m = 1.5$

4 Discussion

In this section a physical interpretation of the grain-size pattern, as found in the model, is given. This is carried out for two hydrodynamic conditions considered in the experiments of the previous section: symmetrical and asymmetrical tidal forcing. The mechanisms discussed here are based on the concepts of the formation of tidal sand ridges under the assumption of uniform sediment, as discussed in Huthnance (1982), Hulscher et al. (1993), Calvete et al. (2001). In addition, the model results are discussed in relation to field observations.

4.1 Symmetrical tidal forcing

The first situation concerns a pure symmetrical M_2 tidal forcing, for which the velocity V of the basic state obeys $\nabla^3 = 0$. This implies that no alongshore sediment flux is present in the basic state and $\mathbf{q}_{b0} = 0$. A local change in the size distribution of the surficial sediment can be understood as a result of the interaction of the tidal current with the bottom. The difference in the sediment transport capacity of the two grain-size classes, caused by hiding effects, reduces the erosion and deposition flux of the finest sediment fraction. Consequently, a fining of the sediment in the erosion areas and a sediment coarsening in the deposition areas occur. A symmetrical current causes only growth of the perturbations and (almost) no migration, because the largest erosion takes place in the troughs and the largest deposition occurs on the crest of the ridges. This corresponds to a mean grain size pattern that is 180° out of phase with the topography. A more quantitative way to understand the results is to examine the equations for the evolution of the bottom. Using Eq. (9) and an M_2 tidal forcing, Eqs. (11) and (12) reduce to

$$(1-p) \frac{\partial h}{\partial t} = -T_2 \nabla \cdot \overline{\mathbf{q}}_b \quad (13)$$

$$(1-p)L_{a0} \frac{\partial f_1}{\partial t} = -T_3 \nabla \cdot \overline{\mathbf{q}}_b, \quad (14)$$

where

$$T_2 = F_1 G_{b1} + F_2 G_{b2} \quad T_3 = F_1 F_2 (G_{b1} - G_{b2}) .$$

The form of the equations is identical, so that the relation between h and f_1 is given by

$$\frac{\partial h}{\partial t} = L_{a0} \left(\frac{T_2}{T_3} \right) \frac{\partial f_1}{\partial t} .$$

Depending upon the sign of the coefficient T_3 , a phase difference between the bottom topography and the spatial pattern of the fraction of fine grains of 0° or 180° is found. The latter case, with the finest sediment on top of the ridges, occurs for $T_3 < 0$, which means $G_{b1} < G_{b2}$, thus $c_b > 0$ (see Fig. 4a).

The enhanced growth rates for bimodal mixtures, compared to uniform sediment, are derived from Eq. (13). In the case of a sediment mixture, the time evolution of the bottom topography differs from that of the uniform sediment case only by a factor T_2 . For a hiding formulation as introduced in Eq. (10), the function $T_2 \geq 1$, leading to the enhanced growth of perturbations for a bimodal sediment mixture. This effect was illustrated in Fig. 3a.

4.2 Asymmetrical tidal forcing

The second case involves forcing by an asymmetrical tidal current, which can be either due to a steady component or the combination of an M_2 and M_4 tide. The important difference with the previous case is the non-zero alongshore bed load flux, in the basic state. This induces a migration of the ridges, in the direction of the maximum tidal current. In turn, the sediment pattern is shifted alongshore with respect to the pattern found for the case of a symmetrical tidal current. In particular, a fining on the (erosive) upcurrent flank of the ridge is found (Fig. 4b), instead of a fining in the trough. Eqs. (11) and (12) in the case of an additional current contribution (\overline{V}_{M_4} or \overline{V}_0) read

$$(1-p) \frac{\partial h}{\partial t} = -T_2 \nabla \cdot \overline{\mathbf{q}}_b - [T_1 + T_2 T_5] \nabla \cdot \overline{(\mathbf{q}_{b0} f_1)} \quad (15)$$

$$0 = -T_3 \nabla \cdot \overline{\mathbf{q}}_b - [T_4 + T_3 T_5] \nabla \cdot \overline{(\mathbf{q}_{b0} f_1)}, \quad (16)$$

where

$$T_1 = G_{b1} - G_{b2} \quad T_4 = F_2 G_{b1} + F_1 G_{b2} \quad T_5 = \frac{c_b \sigma_0 \ln 2}{\sqrt{F_2 F_1}} .$$

The left-hand side of Eq. (12) is neglected. This because the dominant balance is between the terms in Eq. (16) representing the difference in erosion of fine and coarse sediment due to hiding effects and a redistribution of sediment due to the presence of a non-zero background sediment flux. This is a crucial difference with the balance found in the symmetrical tide case.

In the expression for the divergence of the perturbed sediment flux (see Appendix), the term involving the

cross-shore gradient in the cross-shore component of the current ($\partial u'/\partial x$) controls the growth of tidal sand ridges Calvete et al. (2001). The divergence of this flux can thus be approximated by

$$\nabla \cdot \bar{\mathbf{q}}'_b \sim -2\bar{V}^2 \frac{\partial \bar{u}'}{\partial x} + 3 \frac{\bar{V}^3}{H} \frac{h}{\partial y}. \quad (17)$$

Here, the second contribution on the right-hand side causes the migration of the bedforms. To establish the relationship between \bar{h} and f_1 , a flood-dominant current is considered, i.e., $\bar{V}^3 < 0$. For a realistic ratio of the tidal current amplitudes V_{M_4}/V_{M_2} , the first term in the above expression is dominant over the contribution of the migration, reducing Eq. (16) to

$$(T_4 + T_3 T_5) \bar{V}^3 \frac{\partial f_1}{\partial y} \propto T_3 \bar{V}^2 \frac{\partial \bar{u}'}{\partial x}.$$

For realistic values of the standard deviation σ_0 , it is found that $T_4 + T_3 T_5 > 0$. The perturbed residual velocity follows the bottom contours, with an offshore component on the seaward flank of the ridge and a landward component on the landward flank, resulting in a clockwise (anticyclonic) circulation around the bank, leading to $\partial \bar{u}'/\partial x \propto h$. If this is substituted in the expression above, it follows that

$$-\frac{\partial f_1}{\partial y} \propto (G_{b1} - G_{b2})h$$

and the size distribution is 90° out of phase with topography. If $c_b > 0$, then $G_{b1} < 1 < G_{b2}$ and a fining of the bottom sediment on the upcurrent (seaward) flank of the ridges occurs. In Fig. 4b this case is shown, where the phase shift is less than 90° ; this is due to the additional contribution of the migration term in Eq. (17).

The enhanced growth and migration rates for bimodal mixtures, compared to uniform sediment for asymmetric tides, are due to the same effects as those discussed in case of a symmetrical tidal forcing. The main difference between these two cases is the last term (redistribution of sediment) in Eq. (15). However, experiments indicate that this contribution is of only minor importance to the growth and migration of the tidal sand ridges.

4.3 Comparison with field observations

The model predicts tidal sand ridges with the crest rotated cyclonically at an angle of $30^\circ - 35^\circ$ with the tidal current axis, which is in good agreement with measurements (Vincent et al. 1998). Forcing the model with a symmetrical M_2 tide showed that the coarsest sediment is located on the crest of the ridges, consistent with the general trend that is detected in the field data of the Belgium shelf. Furthermore, if an external forcing by a flood-dominant tidal current is considered, hiding effects in the bed load transport result in a pattern of the mean grain-size that is comparable to that observed on the southern part of the Middelkerke Bank, i.e. with the

coarsest sediment on the landward flank. The perturbed velocity results in an anticyclonic circulation around the bank, with on the landward flank a residual velocity component in the ebb direction. It should be noted that the eastern flank, where the coarser sediments are found, corresponds to a large dune area of which the asymmetry indicates an ebb dominance (Lanckneus et al. 1994). According to the model results, the offshore decrease in the flood dominance contributes to the shift in the location of the maximum mean grain size. It is found that, for a temporal phase between the M_2 and M_4 tidal constituents such that the residual sediment flux is in the ebb direction, the coarsest sediment is located on the seaward flank. This is in accordance with the pattern found on the northern end of the bank. The internal structure of the Middelkerke Bank indicates a long-term migration, although its present situation remains unclear (Berné et al. 1994). The model for the flood-dominated tidal current predicts the opposite pattern. An along-shore migration, leading to erosion on the seaward flank, is obtained.

Other researchers have suggested that the shift in the pattern could be related to the steepness of the flanks of the ridges. In the direction perpendicular to their main axes, the profile of the ridges is asymmetrical, with a steep seaward flank (Lanckneus et al. 1994). Since in the present study a linear stability approach is used, only symmetrical (sinusoidal) perturbations were incorporated into the model; thus this particular hypothesis cannot be verified. Further research with a non-linear model could provide such information.

The influence of storms on tidal sand ridges and their sedimentary pattern is still a matter of debate. As banks may rise up to 4 m below low water level at spring tide, the small depths and the exposure to storm waves from the north renders them susceptible to waves. Vincent et al. (1998) pointed out that the combined effect of strong tidal flows and oscillatory wave-induced currents, acting approximately normal to the tide, mainly results in the (enhanced) resuspension of the bottom sediment. However, no observable effect on the direction of transport was found. The bank volume was used by Lanckneus et al. (1994) to assess the impact of different weather conditions on the formation and maintenance of the Middelkerke Bank. These investigators found that the bank volume decays in periods of winter storms, whilst the bank is restored during extended periods of fair weather. Despite large variations of the volume during the season, these data suggest that in the long-term the banks are in equilibrium with the hydrodynamic conditions. On the other hand, Vincent et al. (1998) presented data which show an upslope sediment transport during storms. This pattern suggests that waves are important for the maintenance of the ridges, not only acting to prevent their unrestricted growth due to tidal currents alone. Besides the impact on the morphology, Houthuys et al. (1994) focused also upon the effect of storms on the surficial sediment grain-size. Quiescent, prestorm

conditions (fair weather), which are supposed to represent the tidally forced equilibrium state, were compared with the sediment distribution after a normal autumn storm period. The main changes were a coarsening on the northwestern flank and a fining of the landward flank. It was argued that waves coming from the north cause a winnowing of fine sediment on the exposed seaward flank, with subsequent deposition on the landward flank. In short, there is no consensus in the literature regarding the influence of storms and waves on the formation of the tidal sand ridges on the Belgian shelf (Houthuys et al. 1994; Vincent et al. 1998). Also, the ratio of suspended load transport over bed load transport is poorly known. The influence of waves was not included in this study, and only bed load transport was accounted for. The largest influence of waves can be expected in the non-linear regime, as is supported by work done by Huthnance (1982), which indicates that the effect of wind waves on the initial growth of tidal ridges is small. This paper explores tidal sand ridges only in the linear regime. Nevertheless, owing to these uncertainties, the application of the results would be more appropriate for tidal sand ridges in deeper water in the southern North Sea. The main problem with this is that no extensive sediment data are available for the more offshore located ridges, so that no verification of the model results is possible.

Including a suspended load transport in a tidally dominated (i.e. fair weather) forcing corresponds to an additional sediment flux, related to a higher power in the flow velocity (see in Bailard 1981). Such a flux would enhance the growth rate and migration speed of the bottom perturbations. It does not change the bottom patterns as presented in this paper, but a grain size-dependent suspended load flux (enhanced transport of fine sediment) could, in principle, reverse the mean grain-size patterns as found for bed load only (reduced transport fines). It would require a suspended load flux of the same order of magnitude as the bed load flux during fair weather and a strong grain-size dependence.

The present model, with the restriction to bed load transport and tidally dominated or fair weather conditions, is not directly applicable to other shelves. Sedimentological information on sand ridges and grain-size distributions exists for the Bristol Channel (Pattiaratchi and Collins 1987) and for tidal sand ridges in the Florida inner shelf (Davis et al. 1993). Although interesting differences with the sorting pattern (e.g. the location of finest and coarsest sediment on ridge topography) for ridges on the Belgium shelf are perceived, a comparison with these data is beyond the scope of the present paper.

5 Conclusions

In this paper, a model was developed and analyzed to study the initial formation of tidal sand ridges and the corresponding grain-size distribution on meso-tidal

shelves. The sediment was transported as bed load and dynamic hiding effects resulted in the selective transport of the two grain-size classes.

The objective of the present study was to gain insight into the physical mechanisms responsible for the observed grain-size distribution over the tidal sand ridges. To this end, the temporal and spatial characteristics of tidal ridges in case of a bimodal sand mixture were compared with results obtained in the case of a single grain-size class. Growth rates and migration velocities increased with increasing standard deviation of the sediment mixture, yielding realistic time scales for the formation of the ridges. The wavelengths of the ridges remained unchanged, if more than one size class was considered. The experiments undertaken have also revealed the importance of different forcing conditions. A forcing by M_2 tidal currents, in combination with a reduced flux of fine grains, resulted in a grain-size distribution which was in phase with the ridge topography. The coarsest mean grain-size was located on the crests, representative of the general pattern of the data. A shift between the topographical pattern and the pattern of mean grain-size was introduced by adding an M_4 tidal constituent or a steady current to the forcing. A flood-dominant tidal current, in combination with the hiding of the finest grains, resulted in a coarser landward flank. These results are in fair agreement with data of offshore tidal sand ridges on the Belgium shelf.

Acknowledgements This research was supported by the Cornelis Lely Foundation in The Netherlands (Delft) and by the EC-MAST 5 HUMOR project (contract nr. EVK3-CT-2000-00037).

Appendix. Sediment flux

$$\mathbf{q}_{b0} = (0, 3v_b V^3)$$

$$\mathbf{q}'_b = \left(v_b \left[3V^2 u' - \lambda_b |V|^3 \frac{\partial h}{\partial x} \right], \right. \\ \left. \pm v_b \left[3V^2 v' - \lambda_b |V|^3 \frac{\partial h}{\partial y} \right] \right)$$

$$\nabla \cdot \mathbf{q}'_b = v_b \left[V^2 \left(\frac{2}{V} \frac{\partial V}{\partial x} - \frac{3}{H} \frac{\partial H}{\partial x} \right) u' - 2V^2 \frac{\partial u'}{\partial x} \right. \\ \left. + 3 \frac{V^3}{H} \frac{\partial h}{\partial y} - \lambda_b |V|^3 \left(\frac{\partial^2 h}{\partial x^2} + \frac{\partial^2 h}{\partial y^2} + \frac{3}{V} \frac{\partial V}{\partial x} \frac{\partial h}{\partial x} \right) \right].$$

Here, the linearized mass conservation is used to eliminate v' in the expression for $\nabla \cdot \mathbf{q}'_b$. It reads:

$$v' \frac{\partial H}{\partial x} = V \frac{\partial h}{\partial y} - H \frac{\partial u'}{\partial x} - u' \frac{\partial H}{\partial x}. \quad (18)$$

References

- Antia EE (1996) Shoreface-connected ridges in German and US Mid-Atlantic bights: similarities and contrasts. *J Coast Res* 12: 141–146

- Bailard J (1981) An energetics total load sediment transport model for a plane sloping beach. *J Geophys Res* 86: 10938–10954
- Berné S, Trentesaux A, Stolk A, Missiaen T, de Batist M (1994) Architecture and long-term evolution of a tidal sandbank: the Middelkerke Bank (southern North Sea). *Mar Geol* 121: 57–72
- Besio G, Blondeaux P, Brocchini M, Vittori G (2003) Migrating sand waves. *Ocean Dynamics* 53, 232–238, doi:10.1007/s10236-003-0043-x.
- Calvete D, Walgreen M, De Swart HE, Falqués A (2001) A model for sand ridges on the shelf: effect of tidal and steady currents. *J Geophys Res* 106 (C5): 9311–9326
- Davis RA, Klay J, Jewell P (1993) Sedimentology and stratigraphy of tidal sand ridges southwest Florida inner shelf. *J Sed Petrol* 63 (1): 91–104
- Dyer KR, Huntley DA (1999) The origin, classification and modelling of sand banks and ridges. *Contin Shelf Res* 19: 1285–1330
- Foti E, Blondeaux P (1995) Sea ripple formation: the heterogenous sediment case. *Coastal Eng* 25: 237–253
- Gao S, Collins MB, Lanckneus J, De Moor G, Van Lancker V, (1994) grain-size trends associated with net sediment transport patterns: an example from the Belgian continental shelf. *Mar Geol* 121: 171–185
- Houthuys R, Trentesaux A, De Wolf P (1994) Storm influences on a tidal sandbank's surface (Middelkerke Bank, southern North Sea). *Mar Geol* 121: 23–41
- Hulscher SJMH, De Swart HE, De Vriend HJ (1993) The generation of offshore tidal sand banks and sand waves. *Contin Shelf Res* 13 (11): 1183–1204
- Huthnance JM (1982) On one mechanism forming linear sand banks. *Estuar Coast Shelf Sci* 14: 79–99
- Lanckneus J, De Moor G, Stolk A (1994) Environmental setting, morphology and volumetric evolution of the Middelkerke Bank (southern North Sea). *Mar Geol* 121: 1–21
- Lanzoni S, Tubino M (1999) Grain sorting and bar instability. *J Fluid Mech* 393: 149–174
- Off T (1963) Rhythmic linear sand bodies caused by tidal currents. *Bull Am Assoc Petrol Geol* 47 (2): 324–341
- Pattiaratchi C, Collins M (1987) Mechanisms for linear sandbank formation and maintenance in relation to dynamical oceanographic observations. *Prog. Oceanogr.* 19: 117–176
- Ribberink JS (1987) Mathematical modelling of one-dimensional morphological changes in rivers with non-uniform sediment. PhD, Thesis, Tech Univ Delft The Netherlands.
- Seminara G (1995) Effect of grain sorting on the formation of bedforms. *Appl Mech Rev* 48 (9): 549–563
- Swift DJP, Parker G, Lanfredi NW, Perillo G, Figge K (1978) Shoreface-connected sand ridges on American and European shelves: a comparison. *Estuar Coast Mar Sci* 7: 257–273
- Trentesaux A, Stolk A, Tessier B, Chamley H (1994) Surficial sedimentology of the Middelkerke Bank (southern North Sea). *Mar Geol* 121: 43–55
- Trentesaux A, Stolk A, Berné S (1999) Sedimentology and stratigraphy of a tidal sand bank in the southern North Sea. *Mar Geol* 159: 253–272
- Van Lancker V (1999) Sediment and morphodynamics of a siliclastic near coastal area, in relation to hydronamical and meteorological conditions: Belgian continental shelf. PhD. Thesis, Univ Gent, Gent, Belgium.
- Vincent CE, Stolk A, Porter CFC (1998) Sand suspension and transport on the Middelkerke Bank (southern North Sea) by storms and tidal currents. *Mar Geol* 150: 113–129
- Walgreen M, Calvete D, De Swart HE (2002) Growth of large-scale bed forms due to storm-driven and tidal currents: a model approach. *Contin Shelf Res* 22 (18–19): 2777–2793
- Walgreen M, De Swart HE, Calvete D (2003) Effect of grain-size sorting on the formation of shoreface-connected sand ridges. *J Geophys Res* 108(C3): 3063, doi:10.1029/2002JC001435.
- Williams JJ, MacDonald NJ, O'Conner BA, Pan S (2000) Offshore sand bank dynamics. *J Mar Sys* 24: 153–173
- Zimmerman JTF (1981) Dynamics, diffusion and geomorphological significance of tidal residual eddies. *Nature* 290: 549–555